Monthly Notices
of the
ROYAL ASTRONOMICAL SOCIETY

MNRAS **486,** 4724–4737 (2019)
Advance Access publication 2019 April 27

doi:10.1093/mnras/stz1156

A simple non-equilibrium feedback model for galaxy-scale star formation: delayed feedback and SFR scatter

Matthew E. Orr [1]★ Christopher C. Hayward [2] and Philip F. Hopkins [1]

[1] *TAPIR, Mailcode 350-17, California Institute of Technology, Pasadena, CA 91125, USA*
[2] *Center for Computational Astrophysics, Flatiron Institute, 162 Fifth Avenue, New York, NY 10010, USA*

Accepted 2019 April 25. Received 2019 April 22; in original form 2018 October 22

ABSTRACT

We explore a class of simple non-equilibrium star formation models within the framework of a feedback-regulated model of the ISM, applicable to kiloparsec-scale resolved star formation relations (e.g. Kennicutt–Schmidt). Combining a Toomre-Q-dependent local star formation efficiency per free-fall time with a model for delayed feedback, we are able to match the normalization and scatter of resolved star formation scaling relations. In particular, this simple model suggests that large (∼dex) variations in star formation rates (SFRs) on kiloparsec scales may be due to the fact that supernova feedback is not instantaneous following star formation. The scatter in SFRs at constant gas surface density in a galaxy then depends on the properties of feedback and when we observe its star-forming regions at various points throughout their collapse/star formation 'cycles'. This has the following important observational consequences: (1) the scatter and normalization of the Kennicutt–Schmidt relation are relatively insensitive to the local (small-scale) star formation efficiency; (2) but gas depletion times and velocity dispersions are; (3) the scatter in and normalization of the Kennicutt–Schmidt relation is a sensitive probe of the feedback time-scale and strength; (4) even in a model where $\tilde{Q}_{\rm gas}$ deterministically dictates star formation locally, time evolution, variation in local conditions (e.g. gas fractions and dynamical times), and variations between galaxies can destroy much of the observable correlation between SFR and $\tilde{Q}_{\rm gas}$ in resolved galaxy surveys. Additionally, this model exhibits large scatter in SFRs at low gas surface densities, in agreement with observations of flat outer H I disc velocity dispersion profiles.

Key words: ISM: evolution – ISM: kinematics and dynamics – galaxies: ISM – galaxies: star formation.

1 INTRODUCTION

One of the fundamental characteristics of star formation is that it is globally inefficient: galaxies convert only a few per cent of their cold gas reservoirs into stars per dynamical time (Kennicutt et al. 2007). As to why this is the case, there are two broad frameworks for regulating star formation in galaxies: dynamics and feedback. Dynamical regulation argues that stars form as rapidly as they are able, but that dynamical processes such as turbulent shear, differential rotation, or gas expansion behind spiral arms govern the fraction of gas with conditions favourable to star formation (Saitoh et al. 2008; Robertson & Goldreich 2012; Elmegreen & Hunter 2015; Semenov, Kravtsov & Gnedin 2017). In this regime, star formation efficiency (SFE) is low locally, in complement with its global value. Feedback regulation argues instead that star formation could be locally highly efficient in regions that are actually collapsing without local feedback present, but that stellar feedback (usually in addition to dynamical processes), in the form of ionizing radiation or supernova explosions, heat and stir the interstellar medium (ISM), preventing further star formation in most regions and times (Thompson, Quataert & Murray 2005; Murray, Quataert & Thompson 2010; Ostriker, McKee & Leroy 2010; Shetty & Ostriker 2012a; Hopkins et al. 2014; Kim & Ostriker 2015b; Hopkins et al. 2018a, among others).

Within the framework of feedback regulation, there have been several related models describing various star formation 'laws', including the 'outer disc' model of Ostriker & Shetty (2011), the 'two-zone' theory of Faucher-Giguere, Quataert & Hopkins (2013), and radiation–pressure-supported models such as Thompson et al. (2005), to name a few. Particular focus has been laid on models involving turbulent support of the ISM, as thermal heating processes become relatively ineffective at regulating star formation for gas surface densities above $\sim 10\,{\rm M}_\odot\,{\rm pc}^{-2}$, where a

★ E-mail: meorr@caltech.edu

self-shielded component of the ISM necessarily develops (Schaye 2004; Krumholz, McKee & Tumlinson 2009a,b; Hayward & Hopkins 2017). Broadly, turbulently regulated models incorporate some metallicity dependence (often having to do with the metallicity dependence of the efficiency of SNe momentum coupling, Martizzi, Faucher-Giguere & Quataert 2015), local gas fraction (or stellar surface density, Ostriker & Shetty 2011), or local gas scale height dependence (Faucher-Giguere et al. 2013), in setting the equilibrium star formation rate (SFR).

These models have found general agreement with the *mean* observed SFRs (either galaxy-integrated or as a function of radius) in nearby galaxies. However, observational studies of the spatially resolved (at ∼kpc scales) Kennicutt–Schmidt relation have apparently characteristic $\pm 2\sigma$ scatters of $\sim 1-2$ dex in SFRs at constant gas surface densities (Bigiel et al. 2008; Leroy et al. 2008; Bigiel et al. 2010; Leroy et al. 2013, 2017), with a similar scatter having been seen in cosmological simulations (Orr et al. 2018). Generally, these variations in SFRs within individual galaxies at constant gas surface density are not readily explained by local variations in metallicity. For instance, at fixed galactocentric radii in discs, gas metallicity is seen to vary at $\lesssim$0.1 dex levels (Ho et al. 2017), whereas gas surface densities can vary by more than 2 dex, requiring SFE $\propto Z^{20}$ (not seen observationally, or having a theoretical basis for being the case) to explain SFR variations independent of gas surface densities. Nor are metallicity gradients large enough to explain the scatter, as generally gas surface densities fall far more quickly than metallicities (Ma et al. 2017). Gas fractions, too, appear lacking in their ability to drive large scatter in SFRs at constant gas surface density *within* galaxies (Leroy et al. 2013).

This large scatter could suggest that we are still missing some critical physics in our models, or observationally our inferred SFRs and gas surface densities are introducing much larger errors than usually appreciated. From the side of theory, where we are roughly matching SFR distributions, and their scatter in particular, in cosmological simulations is heartening (Orr et al. 2018), and suggests the feedback physics included in simulations such as those of Hopkins et al. (2014, 2018a) or Agertz & Kravtsov (2015) is close to sufficient. On the side of observations, there remains work to be done in converging on conversion factors between luminosities or line widths, and SFRs and gas masses but it is unlikely that these factors randomly vary by ∼2 dex in neighbouring kpc-patches of ISM (Kennicutt & Evans 2012; Narayanan et al. 2012; Bolatto, Wolfire & Leroy 2013).

Another possible resolution is that rather than star formation being locked to a 'law' dependent on gas surface density, there is some 'intrinsic' uncertainty to it (Schruba et al. 2010; Calzetti, Liu & Koda 2012; Kruijssen & Longmore 2014; Kruijssen et al. 2018). Kruijssen & Longmore (2014) argue that star formation relations such as that of the Kennicutt–Schmidt relation must necessarily break down on some scale due to the overlap (or lack thereof) both temporally and spatially between tracers of dense gas and star formation, and that scatter in these relations is a necessary consequence. But to what extent does the framework of feedback regulation itself provides an intrinsic scatter to the predicted equilibrium SFRs? After all, feedback is not instantaneous with star formation, as ionizing radiation is injected for upwards of 10 Myr (Leitherer et al. 1999), supernova feedback is not felt for the first ∼5 Myr, and then continues stochastically for ∼30 Myr (Agertz et al. 2013). The time-scales for feedback injection are not coincidentally on the order of the lifetimes of star-forming regions themselves in the feedback regulated model (Oklopčić et al. 2017; Grudić et al. 2018; Semenov, Kravtsov & Gnedin 2018). Star formation *equilibrium* need not be expected, even at the $10^6\,M_\odot$ giant molecular cloud (GMC) scale.

Indeed others (Benincasa et al. 2016; Torrey et al. 2017; Semenov et al. 2018) have argued that while star formation might be in 'static equilibrium' (i.e. steady state) in some averaged sense, it is locally in some *dynamical* equilibrium where the ISM is in a constant cycle of collapse, star formation, and cloud destruction/feedback. It is thus never instantaneously in local equilibrium, and is constantly oscillating between those phases (Benincasa et al. 2016; Semenov et al. 2017, 2018), a fact supported by simulations (Orr et al. 2017; Sparre et al. 2017; Torrey et al. 2017).

In this paper, within the framework of feedback regulation, we explore a simple non-equilibrium star formation model, which expands upon these previous works. Critically, we explore models wherein there is a non-trivial delay time, with respect to the local dynamical time, between the formation of young stars and the injection of the bulk of their feedback into the ISM. We investigate the results of including a time dependence between the criteria for star formation being met, and its effects being felt, in particular, the ability to explain significant (∼dex) scatter in SFRs in resolved galaxy scaling relations. We explore how this ultimately leads to scatter in the Kennicutt–Schmidt relation, but also a number of non-intuitive effects for observed galaxy scalings of quantities that enter the model. For the reader, Table 1 shows a listing of variables and important parameters included in the model and discussed throughout the paper.

2 MODEL

In a previous work (Orr et al. 2018), we explored the ability of turbulent energy injection, in the form of the effects of Type II SNe, to explain the equilibrium value of the Kennicutt–Schmidt relation in the FIRE simulations at gas surface densities $\gtrsim 10\,M_\odot\,pc^{-2}$ (similar in derivation to Ostriker & Shetty 2011; Faucher-Giguere et al. 2013; Hayward & Hopkins 2017). The predicted equilibrium was in good agreement with the median values seen in the simulations, which were themselves in good agreement with the observed atomic + molecular formulation of the Kennicutt–Schmidt relation. However, the $\pm 2\sigma$ scatter seen, on the order of $\sim 1.5-2$ dex, was not fully explained by local environmental variations, e.g. metallicity, dynamical time, or stellar surface density. There appeared to be an intrinsic scatter of $\gtrsim$dex to the SFR distribution seen at any given gas surface density.

To explore the physical processes that cause scatter in resolved star formation scaling relations in disc environments within individual galaxies, let us consider a patch of the ISM where the turbulent velocity dispersion is taken to be roughly isotropic, where we assume

$$\sigma^2 = \sigma_R^2 + \sigma_z^2 + \sigma_\phi^2 \approx 3\sigma_R^2, \tag{1}$$

or $\sigma \approx \sqrt{3}\sigma_R$, where σ is the overall gas velocity dispersion, and the subscripted σ's denote the velocity dispersions in the radial, vertical (i.e. line of sight in face-on galaxies), and tangential directions, respectively.

In the framework of a supersonic turbulent cascade, the largest eddies carry the bulk of the energy and momentum to first order, and we can take the momentum per area in the turbulent/random motion of the gas to be the velocity dispersion at the largest scale (here, the gas disc scale height H) times the gas mass surface density Σ_g, that is $P_{turb} = \Sigma_g \sigma$. The time-scale for the dissipation t_{diss} of this turbulent

momentum[1] is roughly the (twice) eddy turnover time $t_{\rm eddy}$, which is $t_{\rm eddy} \approx H/\sigma_z$. If we assume that the gas disc is embedded in the potential of stellar disc with a larger scale height, as is seen in the Milky Way with the thin gas disc having a characteristic height of $\sim$100 pc embedded within the larger $\sim$300 pc stellar scale height (Gilmore & Reid 1983; Scoville & Sanders 1987), and that the gravitational acceleration near the mid-plane due to the local disc mass itself is of the form $4\pi G\rho_0 z$, where ρ_0 is the mid-plane density (gas + stars), and the external potential[2] introduces a vertical acceleration component of $v_c^2 z/R^2 = \Omega^2 z$ (where $\Omega \equiv v_c/R$), then the vertical (z) density profile is a Gaussian with a characteristic scale height of

$$H = \frac{\sigma_z}{\Omega + \sqrt{4\pi G\rho_0}} \, . \tag{2}$$

So, $t_{\rm diss} \approx 2t_{\rm eddy} \approx 2H/\sigma_z \approx 2/(\Omega + \sqrt{4\pi G\rho_0})$. In the absence of stellar feedback, the turbulent momentum of this patch of the ISM would be expected to exponentially decay as

$$\dot{P}_{\rm turb} = -\Sigma_g \sigma / t_{\rm diss} = -P_{\rm turb}(\Omega + \sqrt{4\pi G\rho_0})/2 \, , \tag{3}$$

which admits a solution for gas velocity dispersions of $\sigma(t) = \sigma_0 \exp(-t(\Omega + \sqrt{4\pi G\rho_0})/2)$.

2.1 Equilibrium model of instantaneous feedback injection in disc environments

However, feedback from massive stars acts to inject momentum back into the ISM at the largest scales (i.e. disc scale heights; Padoan et al. 2016). Taking the characteristic momentum injected per mass of young stars formed to be $P/m_\star$, we can establish an equilibrium for σ if we balance the rate of momentum injection from feedback, $\dot{\Sigma}_\star P/m_\star$, with the turbulence dissipation rate in equation (3), that is,

$$\left(\frac{P}{m_\star}\right)\dot{\Sigma}_\star = \Sigma_{\rm g}\sigma(\Omega + \sqrt{4\pi G\rho_0})/2 \, . \tag{4}$$

Arguing that star-forming discs are marginally stable against gravitational instabilities, we invoke a modified[3] Toomre-Q criterion dictating instantaneous gas stability (Toomre 1964):

$$\tilde{Q}_{\rm gas} = \frac{\sqrt{2}\sigma_R \Omega}{\pi G \Sigma_{\rm disc}} \, , \tag{5}$$

where $\Sigma_{\rm disc} = \Sigma_{\rm g} + \gamma\Sigma_\star$ is the mid-plane surface density, including the stellar component (with the factor γ accounting for the effective fraction of stellar mass within a gas scale height, $\gamma = 1 - \exp(-H/H_\star)$). We substitute this Toomre-Q into equation (4) for σ, recovering the Kennicutt–Schmidt relation for a turbulently supported ISM:

$$\dot{\Sigma}_\star = \pi G \tilde{Q}_{\rm gas}\sqrt{\frac{3}{8}}\frac{\Sigma_{\rm g}\Sigma_{\rm disc}}{P/m_\star}\left(1 + \frac{\sqrt{4\pi G\rho_0}}{\Omega}\right) \, . \tag{6}$$

Further, we can calculate the 'global SFE', i.e. the fraction of the gas mass converted to stars per orbital dynamical time, $\bar{\epsilon}_{\rm sf} \equiv \dot{\Sigma}_\star/\Sigma_g\Omega$, to be

$$\bar{\epsilon}_{\rm sf} = \pi G \tilde{Q}_{\rm gas}\sqrt{\frac{3}{8}}\frac{\Sigma_{\rm disc}(\Omega + \sqrt{4\pi G\rho_0})}{(P/m_\star)\Omega^2} \, . \tag{7}$$

If we take $\tilde{Q}_{\rm gas}$ to be a constant, assuming a value near or slightly below 1, and consider the case in which the disc is not strongly self-gravitating (likely, with the marginal stability of $\tilde{Q}_{\rm gas} \approx 1$), such that $\Omega >> \sqrt{4\pi G\rho_0}$; these two relations boil down to a description of gas surface density and mass fraction and a representation of the ratio of disc surface density to inverse dynamical time, respectively:

$$\dot{\Sigma}_\star = \pi G\sqrt{\frac{3}{8}}\frac{\Sigma_g\Sigma_{\rm disc}}{P/m_\star} \;\; \& \;\; \bar{\epsilon}_{\rm sf} = \pi G\sqrt{\frac{3}{8}}\frac{\Sigma_{\rm disc}}{\Omega P/m_\star} . \tag{8}$$

One deficiency of this model of feedback regulation lies in the calibration of the strength of feedback to isolated Type II SNe simulations (e.g. Kim & Ostriker 2015a; Martizzi et al. 2015). Generally, this overlooks the variation in effective feedback coupling due to the local environment. Especially for predictions regarding the line-of-sight velocity dispersions, the potential saturation or 'venting' of feedback after SNe remnants (superbubbles or otherwise) break out of the disc plane (Fielding et al. 2017, Orr et al. in preparation), or the enhanced momentum injection efficiency of spatially clustered SNe (Gentry et al. 2019), are possible concerns. We do not explore the effects of feedback saturation or SNe (spatial) clustering here, but they warrant further exploration within the framework of simple analytic models (these effects are self-consistently handled in galaxy simulations that resolve gas discs and supernova remnants in the snowplow phase).

2.2 Non-equilibrium model of feedback injection in disc environments

The model derived in Section 2.1 is an equilibrium model, which assumes that feedback injection is statically balanced with the dynamical/dissipation rate. However, we might consider here that the departures from equilibrium occurring on the feedback delay time-scale are important for setting the scatter seen in $\dot{\Sigma}_\star$ at constant $\Sigma_{\rm g}$ in the Kennicutt–Schmidt relation, and at constant $\Sigma_g\Omega$ for the Elmegreen–Silk relation, as well as in σ_z–$\dot{\Sigma}_\star$ space. We will explicitly consider only delayed feedback (i.e. Type II SNe) in this model.[4]

[1] In Faucher-Giguere et al. (2013), they assume that turbulent *energy* dissipates in an eddy crossing time. However, if $E_{\rm turb} \sim P_{\rm turb}^2/2\Sigma_{\rm g}$ and $\Sigma_{\rm g}$ is constant, then $\dot{E}_{\rm turb} \sim P_{\rm turb}\dot{P}_{\rm turb}/\Sigma_{\rm g}$. The exponential turbulent energy dissipation rate $\dot{E}_{\rm turb} \sim -E_{\rm turb}/t_{\rm eddy}$ becomes $P_{\rm turb}\dot{P}_{\rm turb}/\Sigma_g \sim -P_{\rm turb}^2/2\Sigma_g t_{\rm eddy}$, reducing to $\dot{P}_{\rm turb} \sim -P_{\rm turb}/2t_{\rm eddy}$, i.e. that the turbulent *momentum* decays approximately in twice an eddy crossing time. For consistency, and since SNe are momentum-conserving, we adopt a momentum-centric focus throughout the paper.

[2] Here, the local dark matter contribution is implicitly included, whereas it is ignored for simplicity in the disc self-gravity acceleration term as the baryonic component dominates the thin disc mass in galaxies. Our model could be extended to gas-rich dwarfs or high-redshift galaxies with poorly defined discs, but would require a different formulation of gas scale lengths/heights.

[3] This is not the 'real' two component Toomre-Q (Rafikov 2001), but is a much simplified version that is sufficiently accurate for our purposes (using the full two-component Q makes little difference to our numerical calculations but prevents us from writing simple analytic expressions).

[4] Although prompt feedback (e.g. radiation pressure and stellar winds) injects a similar amount of momentum per mass of young stars over their lifetimes (Agertz et al. 2013), the 'characteristic' velocity at which this momentum couples to the ISM on large scales is lower by a factor of 20 or so, compared to SNe feedback (Murray et al. 2010; Faucher-Giguere et al. 2013). As we consider here the ability of feedback to regulate the disc scale properties that regulate star formation 'from the top down', we neglect explicitly treating the prompt feedback effects in our model. Instead, we implicitly incorporate

Rather than holding the turbulent velocity dispersion σ constant in time, we allow it to vary, defining the behaviour of its derivative $\dot{\sigma}$ as

$$\dot{\sigma} = \dot{\sigma}_{\rm SNe} - \sigma/t_{\rm eddy}, \tag{9}$$

where $\dot{\sigma}_{\rm SNe}$ is the term explicitly following the current injection of SNe feedback momentum due to past star formation (see equation 10, next), and the $\sigma/t_{\rm eddy}$ term accounts for the exponential decay of supersonic turbulence on roughly an eddy crossing time (equation 3). We ignore the fraction of turbulent momentum 'locked away' into stars (equivalent to a $\sigma\,\dot{\Sigma}_g$ term) as the term is negligible with the depletion time of gas typically on the order of ∼Gyr in galaxies (Leroy et al. 2008, 2013).

Developing a form for $\dot{\sigma}_{\rm SNe}$, we consider that Type II SNe feedback from a given star formation event is injected after a delay time $t_{\rm d}$, and over a period $\delta t_{\rm d}$, corresponding to the lifetime of the most massive star formed, and the time until the least massive star to undergo core-collapse does so thereafter. Furthermore, convolving the number of stars of a given mass with their lifetimes produces a shallow power-law distribution in time over which SNe occur after a star formation event, such that $\mathrm{d}N_{\rm SNII}/\mathrm{d}t \propto t^{-\alpha}$ (see Appendix A for a more detailed derivation). These quantities, $t_{\rm d}$, $\delta t_{\rm d}$, and α, are reasonably known (see Appendix A), and we adopt fiducial values in this paper of 5 Myr, 30 Myr, and 0.46, respectively. As such, the governing equation for $\dot{\sigma}_{\rm SNe}$ takes the form

$$\Sigma_{\rm g}\dot{\sigma}_{\rm SNe} = (P/m_\star)\chi \int_{t_{\rm d}}^{t_{\rm d}+\delta t_{\rm d}} \frac{\dot{\Sigma}_\star(t-t')}{t'^{\alpha}}\mathrm{d}t', \tag{10}$$

where $P/m_\star$ here is the momentum injected by Type II SNe event per mass of young stars (as opposed to from all sources of feedback as in Section 2.1), and χ is a normalization factor such that for a constant SFR $\dot{\Sigma}_\star$ the equation reduces to $\Sigma_{\rm g}\dot{\sigma}_{\rm SNe} = (P/m_\star)\dot{\Sigma}_\star$. We adopt a fiducial value of $P/m_\star = 3000\,\mathrm{km\,s^{-1}}$ (the same value adopted by the FIRE simulations of Hopkins et al. 2014, 2018b), and explore the effects of varying the strength of SNe feedback in Section 3.1.

It is then necessary to formulate a model for the rate at which star formation proceeds, as a function of the current state of the ISM, as we now consider $\dot{\Sigma}_\star$ to drive $\dot{\sigma}$, rather than being purely in a static equilibrium with the turbulent dissipation.

Taking the large-scale marginal gas stability as a key parameter in setting the current rate of star formation, we invoke a simple 'two-phase' model of the ISM, which is instantaneously dependent on the Toomre-Q parameter of the gas disc. Let us assume that some fraction of the gas is in a star-forming phase $f_{\rm sf}$ (i.e. marginally gravitationally bound gas), with the remaining mass in a non-star-forming phase. As explored analytically by Hopkins (2013), supersonic turbulence drives parcels of gas to randomly walk in log-density space such that a fraction (here, $f_{\rm sf}$) is driven to sufficient densities such that local collapse (i.e. leakage) occurs even if the global value of $\tilde{Q}_{\rm gas}$ exceeds the critical threshold for gravitational instabilities Q_0.[5] Following the rationale of Faucher-Giguere et al. (2013, see their appendix C), adapting the calculations of Hopkins (2013), we argue that the mass fraction of gas susceptible to gravitational collapse ($f_{\rm sf}$), which subsequently would be considered in some stage of 'star-forming', is functionally dependent on Toomre-Q, with an adopted power-law form of

$$f_{\rm sf}(\tilde{Q}_{\rm gas}) = f_{\rm sf}^0 \left(\frac{Q_0}{\tilde{Q}_{\rm gas}}\right)^{\beta}, \tag{11}$$

for values $\tilde{Q}_{\rm gas} > Q_0$, and is a constant $f_{\rm sf}^0$ for $\tilde{Q}_{\rm gas} < Q_0$, where $f_{\rm sf}^0$ is the maximal fraction of gas in the star-forming phase, Q_0 represents the Toomre-Q stability threshold, and β accounts for the 'stiffness' of that threshold. Further, as $\tilde{Q}_{\rm gas}$ evolves (in this model, through evolution purely in σ) smoothly in time, the roll-on (or off, if $\dot{\sigma} > 0$) can also be thought to implicitly parametrize our ignorance in how and at what rate GMCs assemble (for $\dot{\sigma} > 0$, this can approximate ionizing radiation and winds dispersing dense material). In Hopkins (2013), the stiffness of the instability threshold (∼β, here) was inversely dependent on the Mach number $\mathcal{M}$ of the turbulence – intuitive, as larger Mach numbers yield a broader lognormal density distribution, increasing the amount of gas above a given density relative to the mean gas density, hence softening the effective gravitational instability threshold. Here, taking $\mathcal{M} \sim \sigma/c_{\rm s}$, where $c_{\rm s}$ is the speed of sound for ∼300 K molecular gas, and $\tilde{Q}_{\rm gas} \sim$ constant, we thus have $\mathcal{M} \propto \sigma \propto \Sigma_{\rm g}$. And so, in our model at a given gas surface density we adopt a stiffness $\beta = -2\log(\Sigma_{\rm g}/\mathrm{M_\odot pc^{-2}}) + 6$, proportional to the Mach number-dependent stiffness fit by (Faucher-Giguere et al. 2013), and substantiated by the observational findings relating $\Sigma_{\rm g}$ and $\mathcal{M}$ of Federrath et al. (2017).

Arguing that a ∼kpc-sized patch of the ISM likely incorporates a large enough number of $\lesssim$100 pc clouds so as to approach an average behaviour in terms of their individual evolutionary states (Schruba et al. 2010; Calzetti et al. 2012; Kruijssen & Longmore 2014), we then adopt a ∼kpc-scale SFR of

$$\dot{\Sigma}_\star(t) = \langle\epsilon_{\rm sf}\rangle\, f_{\rm sf}(\tilde{Q}_{\rm gas}(t))\Sigma_{\rm g}/t_{\rm eddy}, \tag{12}$$

where $f_{\rm sf}(\tilde{Q}_{\rm gas}(t))\Sigma_{\rm g}$ is the mass of gas in the star-forming state (per area), $\langle\epsilon_{\rm sf}\rangle$ is the average SFE per eddy-crossing time (fiducially, 0.025, in line with cloud-scale efficiencies discussed in Elmegreen 2018), and $t_{\rm eddy}$ is the eddy-crossing time. As the quickest instabilities to grow are at the largest scales, the largest being that of the disc scale height itself, the effective free-fall time of gas at the mid-plane density is equivalent to the eddy crossing time $t_{\rm eddy}$ up to an order unity factor (since $t_{ff} \sim 1/\sqrt{G\rho_0} \sim t_{\rm eddy}$). Again, emphasizing that we defined our efficiency $\langle\epsilon_{\rm sf}\rangle$ (taken to be a constant) as a kpc-scale average quantity, $\langle\epsilon_{\rm sf}\rangle \equiv \left\langle \dot{M}_\star t_{\rm eddy}/M_{\rm GMC}\right\rangle$, where $M_{\rm GMC} = f_{\rm sf}(\tilde{Q}_{\rm gas}(t))M_{\rm g}$. It is analogous to a GMC-scale average SFE, and as such is unable to distinguish between high or low efficiency star formation modes on smaller scales (e.g. efficiencies calculated on the basis of higher density gas tracers such as HCN; Kauffmann et al. 2017; Onus, Krumholz & Federrath 2018).

The fiducial values of the physical quantities and common initial conditions included in the evolution of our model – essentially the behaviour of the PDE for σ, equation (9), are enumerated in Table 2. The initial condition of the gas in the model, in all cases presented here, is taken to be $\tilde{Q}_{\rm gas}(t=0) = Q_0 + 1$ (and its corresponding velocity dispersion σ) for the given $\Sigma_{\rm g}$, embedded within static stellar disc with thin and thick components having scale heights of 350 and 1000 pc, respectively, and a relative mass fraction $f_{\rm thick} \equiv \Sigma_{\rm thick,\star}/(\Sigma_{\rm thick,\star} + \Sigma_{\rm thin,\star}) = 0.33$.

its effects regulating the efficiencies of cloud-scale, <100 pc, star formation in our 'GMC-scale' SFE model (Grudić et al. 2018).

[5]This is just a formal calculation of the lognormal density distribution of gas in supersonic turbulence. It is to say: turbulence is able to dynamically replenish the fraction of gas in a lognormal density distribution that is above some critical threshold for self-gravity and collapse.

Table 1. Summary of variables used in this paper.

Symbol	Definition
$\dot{\Sigma}_\star$	Star formation rate surface density
Σ_g	Total gas surface density
f_{sf}	Gas mass fraction in star-forming phase
f_g	Fraction of disc mass in gas
ρ_0	Disc mid-plane volume mass density
t_d	Delay time-scale for the injection of feedback
δt_d	Period of feedback injection
α	Slope of power law for delay-time distribution of Type II SNe
H	Gas scale height
G	Newtonian gravitational constant
$P/m_\star$	Characteristic feedback momentum per mass of stars formed
t_{eddy}	Eddy (disc scale height) crossing time
$\langle\epsilon_{sf}\rangle$	Average SFE per eddy time (here, GMC-scale average value)
$\bar{\epsilon}_{sf}$	SFE per orbital dynamical time
$\tilde{Q}_{gas}$	Modified Toomre-Q gas stability parameter
Ω	Local orbital dynamical time
σ	Turbulent gas velocity dispersion (3D)

Table 2. Fiducial model parameters and disc conditions.

Parameter	Quantity	Fiducial value
Toomre-Q threshold	Q_0	1.0
Max. star-forming fraction	f_{sf}^0	0.3
Average SF efficiency	$\langle\epsilon_{sf}\rangle$	0.025
Feedback strength	$P/m_\star$	3000 km s^{-1}
Feedback delay time	t_d	5 Myr
Feedback duration	δt_d	30 Myr
Power law slope of Type IISNe delay time distribution	α	0.46
Orbital dynamical time	Ω	35 Gyr^{-1}
Disc gas fraction	f_g	0.33
Stellar thick disc fraction	f_{thick}	0.33
Stellar disc height (thin)	$H_{thin,\star}$	350 pc
Stellar disc height (thick)	$H_{thick,\star}$	1000 pc

2.2.1 *Connecting $\dot{\Sigma}_\star$, Σ_g with Observables*

Except for the nearest star-forming regions, (where young star counts or protostellar cores can be used as proxies), observers rarely have true estimates for the 'instantaneous' SFR of a star-forming region. As such, we must connect our 'instantaneous' SFR with observables such as Hα or infrared (IR) flux, which are used as average measures of star formation over a recent period of time $\sim$2$-$4 Myr. For this reason, when we make attempts to compare with observational star formation relations, we average the instantaneous SFR $\dot{\Sigma}_\star$ over the last 3 Myr (see Appendix B for how our results vary with the averaging window). To compare our gas surface densities with observations, we take our gas mass surface density Σ_g to be the atomic + molecular hydrogen gas, correcting them for Helium mass with a factor of 0.75. In panels where we plot the Kennicutt–Schmidt relation, we compare results of our simple model with resolved Kennicutt–Schmidt observations from Bigiel et al. (2008; the light and dark grey shaded regions in background). We correct the gas surface densities in their data with a variable X_{CO} fit from Narayanan et al. (2012). Where we plot depletion time against gas stability (Toomre-Q), we compare

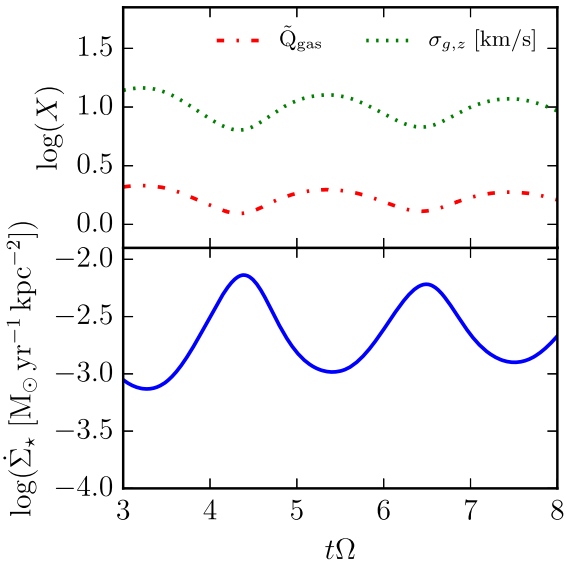

Figure 1. Logarithmic values of star formation rate surface density (the solid blue line; 3-Myr-averaged rate), local $\tilde{Q}_{gas}$ (the dash-dotted red line), and gas velocity dispersion (the dotted green line, units: km s^{-1}) for a period of five dynamical times in our fiducial model gas patch (for fiducial model parameters, see Table 2) with $\Sigma_g = 15$ and $\Sigma_\star = 35\,M_\odot\,pc^{-2}$. The SFR and velocity dispersion maintain stable, albeit slowly decaying, cycles after approximately one dynamical time $\tau_{dyn} \sim \Omega^{-1} \sim 30$ Myr.

with the results of Leroy et al. (2008; the light and dark grey shaded regions in background). For the gas velocity dispersion–SFR panels, we present data from the SAMI IFU survey of kpc-scale resolved observations of star-forming discs of Zhou et al. (2017). As well, we include H I velocity dispersion data of spiral discs from Ianjamasimanana et al. (2015) from the THINGS survey. These data correspond to velocity dispersion–gas surface density observations, lacking direct SFR data. However, given that they are at low gas surface density ($\Sigma_g < 10\,M_\odot\,pc^{-2}$), we take their results to correspond to a range of SFRs for the low gas surface density region in the Bigiel et al. (2008) data set. They are thus presented as a 5$-$12 km s^{-1} band ranging in $\log(\dot{\Sigma}_\star/M_\odot\,yr^{-1}\,kpc^{-2})$ from -2 to -5, constraining the low velocity dispersion, low-SFR region for our models.

3 RESULTS

The simple model produces relatively stable cycles of star formation, inflation, and decay of gas velocity dispersions, and variation in the values of the Toomre-Q parameter, as seen in Fig. 1 for our set of fiducial values of physical parameters, with disc surface densities and conditions chosen to match the solar circle ($\Sigma_g = 15\,M_\odot\,pc^{-2}$, $\Sigma_\star = 35\,M_\odot\,pc^{-2}$, and $\Omega = 35\,Gyr^{-1}$; McKee, Parravano & Hollenbach 2015). As star formation is slow and inefficient (gas depletion times are $\gtrsim$Gyr here), and given the fact that we do not include some gas outflow term, we do not allow Σ_g or $\Sigma_\star$ to vary in the model. And so, $\tilde{Q}_{gas}$ and σ_z are in phase throughout their cycles, by definition since $\tilde{Q}_{gas} \propto \sigma_z$ here, ignoring the relatively weak sigma-dependent γ term in front of $\Sigma_\star$ in Σ_{disc}. Moreover, given the relative stiffness of the star formation threshold in Toomre-Q (for $\Sigma_g = 15\,M_\odot\,pc^{-2}$, the 'stiffness' of $f_{sf}(\tilde{Q}_{gas})$ is $\beta \sim 4.6$), star formation commences and is arrested by feedback before $\tilde{Q}_{gas}$ reaches $Q_0(=1)$, after which the delayed effects of feedback play out, driving $\tilde{Q}_{gas}$ and the velocity dispersions to their maximal

values before the cycle starts anew. The instantaneous SFR (not shown) is nearly completely out of phase with the velocity dispersions and Toomre-Q, rising sharply as $\tilde{Q}_{\rm gas}$ falls and falls nearly as quickly as it rises. The 'observable' quantity, the 3 Myr averaged SFR (c.f. the Hα SFR tracer), shows how the 'observed' SFRs rise by ∼dex as $\tilde{Q}_{\rm gas}$ approaches its minimal value, before falling as the effects of SNe feedback are felt later in the star formation episode.

Variations in the overall strength of feedback, the timing of feedback, and star formation prescription all affect the shape and magnitudes of the star formation cycles in the model, but largely the aforementioned picture holds so long as the time-scale of feedback relative to the dynamical time of the system is short but not effectively instantaneous, and that the magnitude of feedback is insufficient to totally disrupt the system. This therefore applies to both galactic centres and in the outskirts of discs, even where the dynamical time is quite long compared to feedback time-scales, so long as the ISM is turbulently regulated.

Fig. 2 shows the extent of the star formation cycles in the fiducial model across ∼dex in $\Sigma_{\rm g}$ in the Kennicutt–Schmidt, depletion time–stability, and SFR–gas velocity dispersion relations. Results in this figure, and throughout the paper, are plotted as box-and-whiskers in the KS panel that represents the median, interquartile region, and 5–95 per cent data range of individual models run at a given $\Sigma_{\rm g}$. Fig. 2 was run for a range in $\log \Sigma_{\rm g} = 0.8-1.675$ with $\log \Sigma_{\rm g}$ steps of 0.125 dex, all other figures use a range of $\log \Sigma_{\rm g} = 0.8-1.55$ with 0.25 dex $\log \Sigma_{\rm g}$ steps, where $\Sigma_{\rm g}$ is expressed in units of $\rm M_\odot\,pc^{-2}$. Points in other panels (gas velocity dispersion and depletion time–stability relations) are sampled time-steps from those models (seen as clearly separated families of coloured points in the right-hand panel of Fig. 2).

At low $\Sigma_{\rm g}$, the model exhibits increasingly large scatter[6] as the effects of feedback from peak SFRs contribute significantly to the overall momentum budget of the disc (c.f. Section 4.2), producing a larger scatter to in SFRs for KS, and a spur to long depletion times and 'high' Toomre-Qs. In σ–$\dot{\Sigma}_\star$ space, this is seen as a flattening of the relation, covering broad ranges in $\dot{\Sigma}_\star$ with little change in σ. This is broadly in agreement with observations of H I discs in galaxy outskirts having flat velocity dispersion profiles (Ianjamasimanana et al. 2012, 2015). The large velocity dispersions in gas seen above $\dot{\Sigma}_\star \approx 10^{-2}\,\rm M_\odot\,yr^{-1}\,kpc^{-2}$ reflect the fact that feedback is simultaneously able to drive outflows and turbulence in the cold ISM at these SFRs (Hayward & Hopkins 2017). However, in a multiphase ISM, these high dispersions σ_z would not appear in the cold ISM turbulence as this feedback would instead drive outflows (and thus dispersions in the warm neutral and ionized gas components).

Counter-intuitively – but of central importance to observers – when this model is applied to galaxies as a whole (i.e. many $\lesssim$ kpc patches), the relatively tight correlation between Toomre-Q (or gas σ_z) and resolved SFRs within individually evolving patches may be smoothed out by variations in, e.g. local gas fractions, dynamical times, star formation efficiencies, or strength of feedback (i.e. the amount of momentum *coupled* into the cold phase of the ISM per mass of young stars), which may shift subsets of the distribution (c.f. later sections of this paper), effectively widening it on galaxy scales to the relatively broad distribution observed by Leroy et al. (2008). This argument holding for $\dot{\Sigma}_\star \lesssim 10^{-2}\,\rm M_\odot\,yr^{-1}\,kpc^{-2}$, above which outflows would be possible, the presence of which may affect interpretations of distributions in depletion time–Toomre-Q (and σ_z here would no longer strictly encapsulate turbulence in the cold ISM; Hayward & Hopkins 2017).

[6]Regions in an 'off'/low-SFR mode of the cycle may likely be counted as entirely non-star forming in observations, dependent on flux thresholds, given their very low SFRs.

3.1 Variations in the strength and timing of feedback

Fig. 3 explores the effects on this model due to variations in the strength, delay time, and duration of feedback.

3.1.1 Feedback strength P/m$_\star$

The left-hand column of Fig. 3 shows the effects of varying the overall strength of feedback, $P/m_\star$, in our fiducial model: We plot both the Kennicutt–Schmidt relation (relating gas mass and SFR surface densities) and the gas velocity dispersion–SFR relation. As demonstrated extensively in previous works exploring the feedback-regulated regime, variation in the overall strength of feedback primarily affects the equilibrium SFRs where gas self-regulates: stronger (weaker) feedback yields lower (higher) overall SFRs (Hopkins, Quataert & Murray 2011, 2012; Shetty & Ostriker 2012b; Agertz et al. 2013; Hopkins et al. 2014; Orr et al. 2018). By construction, this model follows this paradigm. Interestingly, stronger feedback (per mass of young stars) appears to result in smaller scatter in SFRs. As the star formation time-scales, and the absolute magnitude of momentum injected by feedback, are held roughly constant between models, this can be explained as keeping the relative variance in turbulence constant across the star formation cycles. Hence, if $\Delta\sigma \propto P/m_\star \Delta\dot{\Sigma}_\star$, stronger feedback produces smaller variance in turbulence for smaller variance in $\dot{\Sigma}_\star$.

At low SFRs, the model is not strongly constrained to high or low feedback strengths by the spiral galaxy H I velocity dispersion data set of the THINGS survey (Ianjamasimanana et al. 2015). However, the higher SFR, higher velocity dispersion data from Zhou et al. (2017) do constrain this model in the $P/m_\star \sim 3000-6000\,\rm km\,s^{-1}$ range.

3.1.2 Feedback delay time t$_{\rm d}$ *and duration* δt$_{\rm d}$

The middle and right-hand columns of Fig. 3 show the effects of varying the delay time-scale $t_{\rm d}$ for the first SN feedback (i.e. the lifetime of the most massive star formed in a star formation event, plus the time required to propagate the SNe remnant into the ISM and drive turbulence), and the duration of SN feedback $\delta t_{\rm d}$ (i.e. the difference in stellar lifetimes between the least and most massive stars to undergo a Type II SN in a star formation event). The scatter in SFRs is directly affected by the delay time $t_{\rm d}$, with shorter delays producing less scatter in SFRs. Longer delay times allow for gas to overproduce stars to a greater extent before feedback is felt, hence larger departures from star formation equilibrium. Physically reasonable values of $t_{\rm d} \sim 4-6$ Myr, with a $t^{-0.46}$ weighting, are generally capable of driving $\gtrsim$dex variations in SFRs.

In a similar vein, shorter feedback durations, $\delta t_{\rm d}$, cause effectively burstier overall feedback and, as such, drive larger scatters in SFRs. For reasonable feedback durations of ∼30 Myr (roughly the difference between the lifetimes of an 8 and 40 $\rm M_\odot$ star), the model converges on ∼dex scatter in SFRs. Longer durations smooth out feedback to the extent that it is equivalent in effect to lowering the overall strength of feedback $P/m_\star$.

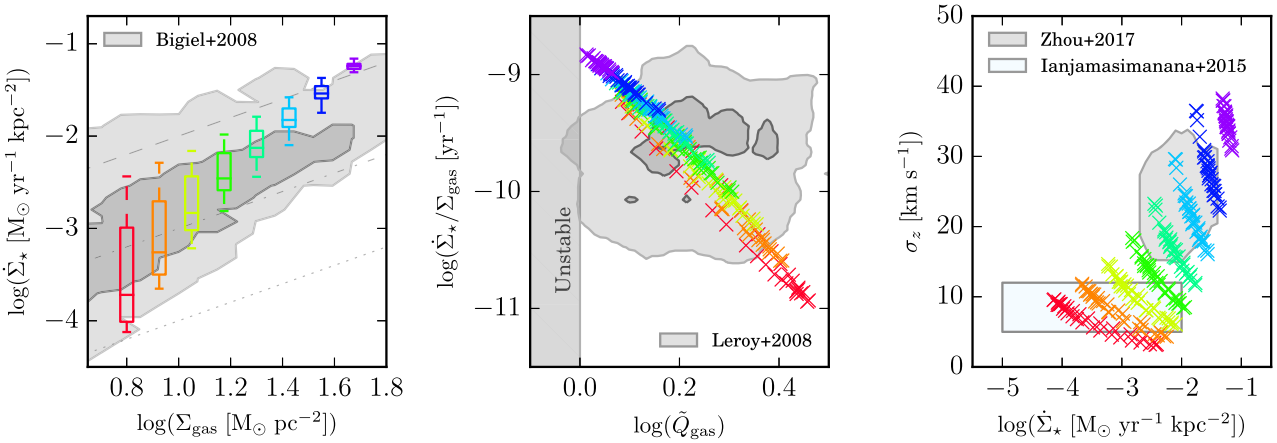

Figure 2. Fiducial model Kennicutt–Schmidt **(left)**, gas depletion time–Toomre-Q **(middle)**, and gas velocity dispersion–SFR **(right)** relations for the fiducial parameters listed in Table 2. The shaded regions in the background represent observational data ranges (c.f. Section 2.2.1) from Bigiel et al. 2008 (left-hand panel), Leroy et al. 2008 (centre panel), and Ianjamasimanana et al. 2015 and Zhou et al. 2017 (the light blue and grey, respectively, right-hand panel). The dashed, dot–dashed, and dotted lines in the KS panel indicate constant depletion times of 10^9, 10^{10}, and 10^{11} yr, respectively. The hatched grey shaded region to the left in the middle panel denotes the Toomre-unstable region. The fiducial model exhibits good agreement with observations of Kennicutt–Schmidt and gas velocity dispersions. The Q-threshold is sufficiently soft with its $f_{\mathrm{sf}}(\tilde{Q}_{\mathrm{gas}})$ 'leakage' to allow star formation to reverse collapse before reaching Q_0/disc instability itself. The upturn in σ_z–SFR above $\dot{\Sigma}_\star \approx 10^{-2}\,\mathrm{M}_\odot\,\mathrm{yr}^{-1}\,\mathrm{kpc}^{-2}$ reflects the fact that feedback from individual star formation events injects a smaller fraction of the overall ISM turbulent momentum and thus is less effective at changing the gravitationally unstable fraction of the ISM (especially true, given that the model lacks outflows to remove gas).

3.2 Variations in star formation rate model

To bake a strüdel, one must first cook the filling. Analogously, in order to generate stellar feedback in a model, one must first produce stars. The local SFR implemented in this model, equation (12), has two principle components that we investigate. Namely, the gas fraction in the star-forming phase $f_{\mathrm{sf}}(\tilde{Q}_{\mathrm{gas}}; Q_0, f_{\mathrm{sf}}^0, \beta)$ (equation 11), and the average local SFE per free-fall time $\langle\epsilon_{\mathrm{sf}}\rangle$.

Varying the star formation model (i.e. the local efficiency of star formation and the Toomre-Q threshold for the onset of gravitational fragmentation/star formation) has larger systematic effects on the results of our model in depletion time–stability space compared to the effects of reasonable variations in the feedback implemented demonstrated in the previous subsection.

3.2.1 Toomre-Q threshold for star formation Q_0

The left-hand column of Fig. 4 demonstrates the effects of the particular choice of the Toomre-Q threshold Q_0 on the Kennicutt–Schmidt and depletion time–Toomre-Q relations. For physically reasonable values, the threshold sets the values of the equilibrium velocity dispersions that the models oscillate about and thus the average magnitude of turbulent momentum in ISM. Along with the overall strength of feedback, the value of the gravitational instabilities threshold is the parameter that most strongly affects the normalization of the Kennicutt–Schmidt relation in our model.

Larger values of Q_0 produce less scatter in the Kennicutt–Schmidt relation, as Q_0 sets the overall amount of turbulent momentum in the ISM ($P_{\mathrm{turb},0} \sim \Sigma_{\mathrm{g}}\sigma(\tilde{Q}_{\mathrm{gas}} = Q_0)$), where star formation occurs and thus dictates the extent to which star formation events can perturb the ISM at a given Σ_{g} (see Section 4.2 for more rationale). When $Q_0 = 0.5$, the model breaks down, as feedback is able to at least double the momentum in the ISM after every star formation episode. For values of Q_0 where the model holds reasonably well ($Q_0 \gtrsim 1$), doubling $Q_0 = 1 \rightarrow 2$ produces an expected $\sim$0.3 dex shift in the Toomre-Q distribution without greatly affecting depletion times (beyond a slight tightening of the SFR distribution): gas is still able to self-regulate (c.f. the predictions of Krumholz & Burkhart 2016).

As $Q_0 \approx 1$ is a physically motivated value for the local gravitational stability threshold of the ISM (Toomre 1964), and that other similar formulations of stability parameters differ only by an order-unity factor in their thresholds for gravitational fragmentation (Rafikov 2001; Kim & Ostriker 2007), we explore only a range in Q_0 of 0.5−2. Generally speaking, this is not a new constraint on Q_0, but rather shows the physical effect of varying the equilibrium level of turbulence on this non-equilibrium model (a 'robustness check' of sorts).

3.2.2 Variations in the maximum star-forming fraction f_{sf}^0

In this model, we consider that at the onset of disc scale height gravitational instabilities ($\tilde{Q}_{\mathrm{gas}} = Q_0$), there is a maximum mass fraction f_{sf}^0 of the ISM participating in star formation. Such a constant has been adopted before in analytic models of feedback regulation in discs (Faucher-Giguere et al. 2013). As seen in the middle column of Fig. 4, we see that so long as this factor f_{sf}^0 does not 'choke' the fraction of material in the star-forming phase, variations have rather small effects qualitatively. This 'choking' appears to occur at high gas surface densities where choices of small maximal fractions $\sim$0.1 clip the maximum SFRs achieved, whereas larger values of f_{sf} do not appear to be the limiting factor on setting maximal SFRs (see the abrupt flattening of $f_{\mathrm{sf}}^0 = 0.1$ points in Fig. 4 at short depletion times). Larger values of f_{sf}^0 move the distributions in depletion time–stability space to shorter depletion times and higher Toomre-Q values; this is the result of renormalizing the 'leakage' curve the model follows as $\tilde{Q}_{\mathrm{gas}}$ evolves (equation 11).

3.2.3 Variations in instantaneous star formation efficiency $\langle\epsilon_{sf}\rangle$

The right-hand column of Fig. 4 shows how variations from $\langle\epsilon_{\mathrm{sf}}\rangle = 0.01$ to $\langle\epsilon_{\mathrm{sf}}\rangle = 0.1$, motivated by observational bounds (Lee, Miville-

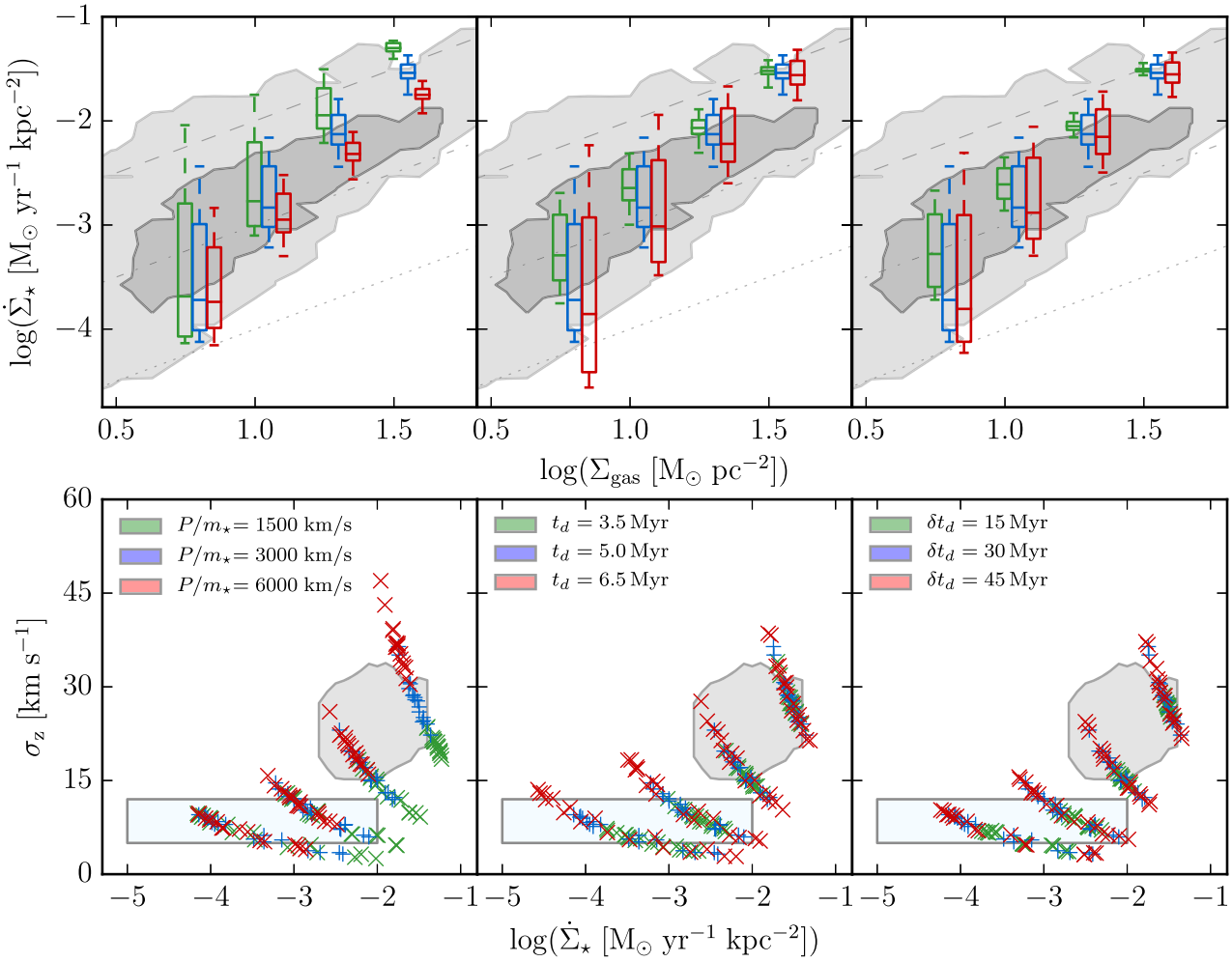

Figure 3. Effects on the Kennicutt–Schmidt **(top row)** and gas velocity dispersion–SFR **(bottom row)** relations due to variations **(columns)** in the overall strength ($P/m_\star$), delay time ($t_{\rm d}$) and duration ($\delta t_{\rm d}$) of SNe feedback in the fiducial model for $3 < t\Omega < 8$. The background shaded regions (observations) and the dashed lines (constant depletion times) are in the style of Fig. 2. **(Top row)** Box-and-whiskers for the model at a given $\Sigma_{\rm g}$ are offset from the central value to show differences between model parameters; **(bottom row)** the coloured points are sampled time-points from models at a given $\Sigma_{\rm g}$, but no offsets are introduced. **(Left)** Raising (lowering) the overall strength of feedback per mass of stars formed, $P/m_\star$, systematically lowers (raises) the peak/integrated star formation rates in the KS relation and raises (lowers) the gas velocity dispersion distribution at a given $\dot{\Sigma}_\star$. Scatter in SFRs is also inversely affected. **(Middle)** The delay time-scale before the first SNe feedback is injected, $t_{\rm d}$, is a strong factor in determining the departures from SF equilibrium and their magnitudes. Longer delays produce larger departures from equilibrium. **(Right)** Varying the period over which SNe momentum is injected by a single stellar population, $\delta t_{\rm d}$, affects the responsiveness of feedback to local ISM conditions. Longer durations weaken the ability of feedback to respond quickly to the ISM conditions, resulting in more scatter in SFRs at constant $\Sigma_{\rm g}$.

Deschênes & Murray 2016), affect the Kennicutt–Schmidt relation, and gas depletion times and stability (Toomre-Q). Interestingly, variations in the local efficiency over a dex change the maximal SFRs by $\lesssim$0.5 dex. In the feedback-regulated regime,[7] so long as the local efficiency factor is above that required to produce *enough* stars to inject the appropriate amount of feedback in the ISM to achieve equilibrium, $\langle\epsilon_{\rm sf}\rangle$ should not affect the large-scale, time-averaged SFRs. However, lower star formation efficiencies do mean that gas must collapse to higher surface densities (i.e. reduced free-fall times) to counteract smaller local efficiencies in order to maintain the momentum balance. More, as the gas collapses further, but does not produce more momentum in feedback overall (to first order), the distributions in depletion time–stability space shift, requiring a less stable ISM generally to support the same SFRs with lower star formation efficiencies (moving by $\sim$0.3 dex in $\tilde{Q}_{\rm gas}$ for a dex change in $\langle\epsilon_{\rm sf}\rangle$).

Though the effect appears less pronounced at high $\Sigma_{\rm g}$, for $\Sigma_{\rm g} \lesssim 10\,\mathrm{M}_\odot\,\mathrm{pc}^{-2}$, lower local star formation efficiencies produce larger scatter in SFRs. This is in part due to the increasing steepness of the unstable gas fraction $f_{\rm sf}(\tilde{Q}_{\rm gas})$, and the ability of gas to overshoot equilibrium SFRs as the arresting effects of feedback are not felt in sufficient amounts at higher velocity dispersions (i.e. larger $\tilde{Q}_{\rm gas}$'s).

Given the degeneracy of the effects of variations in local SFE and the strength, delay and duration of feedback, on the Kennicutt–Schmidt relation, that relation may not be a sensitive probe of smaller scale SFE. Instead, observations in depletion time–stability (Toomre-Q) space have a greater ability to distinguish between low and high local star formation efficiencies in the framework of

[7] See Semenov et al. (2018) for a recent discussion of the relative differences between feedback-regulated and dynamics-regulated star formation.

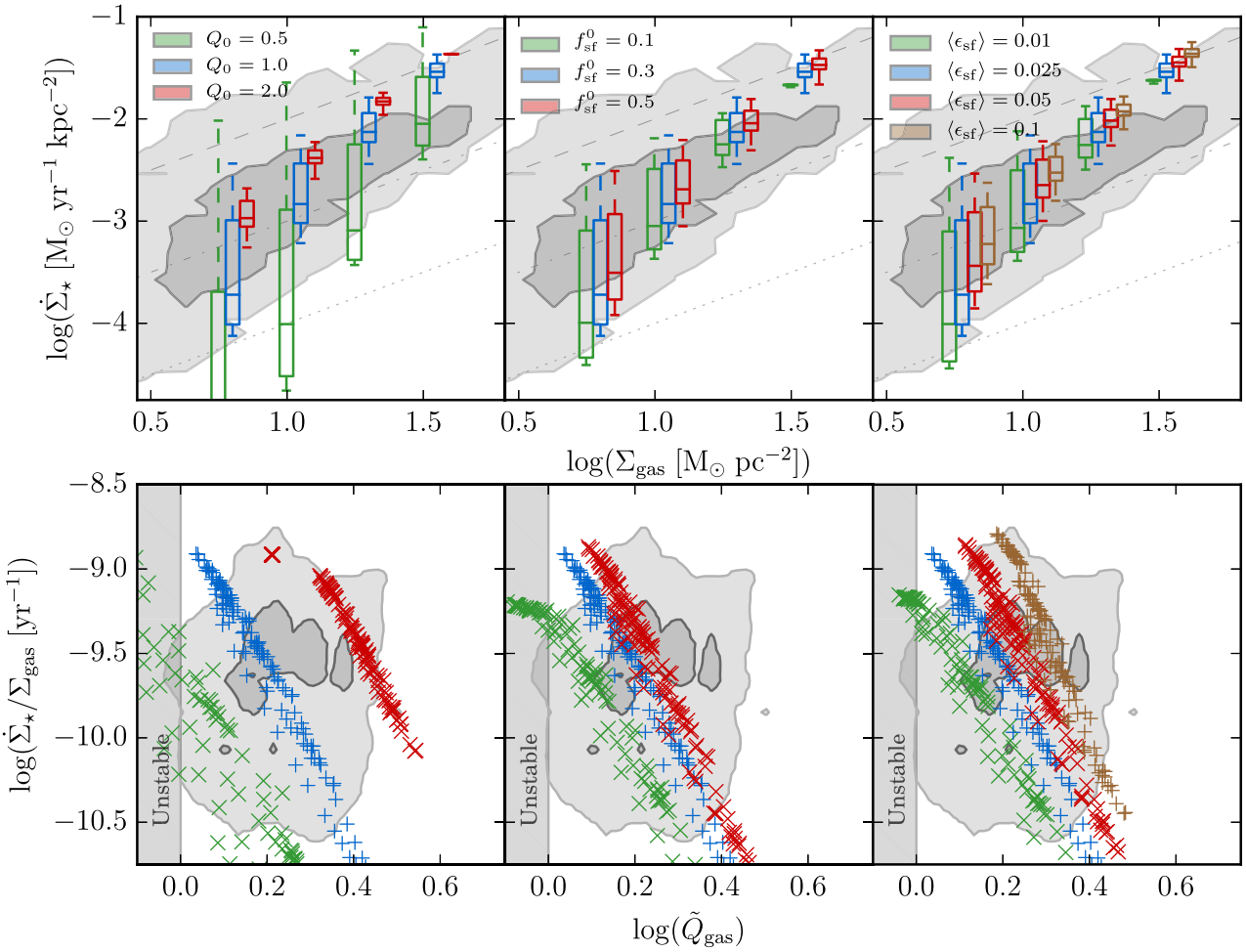

Figure 4. Effects on the Kennicutt–Schmidt **(top row)** and depletion time–stability **(bottom row)** relations due to variations **(columns)** in the Toomre-Q threshold (Q_0), maximal star-forming phase fraction ($f_{\rm sf}^0$), and average local star formation efficiency ($\langle\epsilon_{\rm sf}\rangle$). Plotted quantities and observational data regions are in the style of Fig. 3. **(Left)** Shifting $Q_0 = 1 \rightarrow 2$ moves the distributions in depletion time–stability space by ∼0.3 dex, effectively renormalizing the velocity dispersions for an otherwise-constant KS relations. The scatter in SFR grows with smaller Q_0; as feedback injection accounts for a larger fraction of the ISM momentum budget (normalized by Q_0), and star formation episodes are less stable cycles than explosive events (see Section 4.2). **(Middle)** Varying the maximum fraction of gas in the star-forming phase $f_{\rm sf}^0$ is largely unimportant to the KS relation, as long as it does not 'choke' the amount of gas that would otherwise enter the star-forming phase, but shifts distributions in depletion time–stability space: lower maximum star-forming fractions require lower values of $\tilde{Q}_{\rm gas}$ (i.e. higher gas densities) to achieve the same SFR. **(Right)** Higher local star formation efficiencies $\langle\epsilon_{\rm sf}\rangle$ steepen the peak SFRs in the KS relation and shift the distributions in depletion time–stability space (higher efficiencies mean smaller quantities of unstable gas yield the same SFR), and appear to reduce scatter in KS.

feedback regulation. Given the definitional difficulties of a SFE in this model (i.e. that $f_{\rm sf}$ and $\langle\epsilon_{\rm sf}\rangle$ could be defined together), measurements of the depletion time–stability relation *in similar patches* of the ISM may be useful in quantifying 'the maximally participating fraction' of the ISM in star formation events. To that end, given our fiducial assumption of $f_{\rm sf} = 0.3$, our model favours low cloud-scale average star formation efficiencies $\langle\epsilon_{\rm sf}\rangle \sim 0.01{-}0.1$, as the depletion time–stability constraints otherwise exclude $\langle\epsilon_{\rm sf}\rangle \gtrsim 0.1$ for our fiducial model.

3.3 Reproducing resolved galaxy relations

So far we have considered the star formation cycles of only individual patches of gas. Given that local galaxies ($z \lesssim 0.1$), unlike their high-z progenitors, cannot be modelled as a single star-forming H II region, we build a snapshot of a star-forming galaxy with our model by sampling many patches of a gas disc to understand the global distribution of SFRs and velocity dispersions. We consider here a few exponential discs of gas and stars. Table 3 summarizes the properties of these toy galaxies. We then discretize these discs into Cartesian grids of 750 pc-sized pixels, extending 24 kpc on a side, sampling their surface densities at their centres. For each of these points, we run our model with our fiducial parameters (see Table 2), except for the cases where we have varied the small-scale SFE $\langle\epsilon_{\rm sf}\rangle$, and randomly sample one time-step to find our SFRs, gas surface densities, and velocity dispersions. In two cases here, to highlight galaxy to galaxy variation in GMC properties, we have chosen to vary the small-scale SFE within the bounds of observations (Lee et al. 2016). Ignored here, too, is the variance in $\Sigma_{\rm g}$ at constant radius (e.g. spiral arm features) that may contribute to variance in SFE (Gallagher et al. 2018). The results of this are seen in Fig. 5, where we plot the resulting Kennicutt–Schmidt, gas velocity dispersion–SFR, and depletion time–Toomre-Q relations. We compare our model mock galaxy distributions (light & dark

Table 3. Properties of Mock Galaxies for Fig. 5.

Mock Galaxy	$\Sigma_{g,0}$ ($M_\odot$ pc^{-2})	$\Sigma_{\star,0}$ ($M_\odot$ pc^{-2})	R_g (kpc)	v_c (km s^{-1})	$\langle\epsilon_{sf}\rangle$
Blue	100	1000	6	300	0.01
Green	50	500	6	300	0.025
Red	125	800	10	275	0.025
Purple	125	1000	6	290	0.075

Notes: $\Sigma_{g,0}$ & $\Sigma_{\star,0}$ are central gas and stellar surface densities for exponential discs, with scale lengths R_g & $R_\star$. $R_\star = 3$ kpc for all mock galaxies. v_c is the (flat) circular velocity, used for $\Omega = v_c/R$. $\langle\epsilon_{sf}\rangle$ is varied within observational bounds ∼0.01−0.1 (Lee et al. 2016).

coloured shaded regions) with resolved galaxy observations like previous figures, and find good agreement between this simple model and data. To enable comparison, the central surface densities, scale-lengths, and orbital velocities used in our mock galaxy model were chosen to be comparable with Milky Way-mass spiral star-forming galaxies. We do not plot pixels in our model with $R < 5$ kpc, as these regions are unlikely to be modelled correctly as independent patches following cycles in SFR-gas velocity dispersion space (c.f. the central molecular zone of the Milky Way), given the omission of various dynamical effects such as gas migration and cloud–cloud collisions (Semenov et al. 2017, 2018).

The Kennicutt–Schmidt relation produced by our models in this way finds good agreement with the 'regulated disc' regime of Bigiel et al. (2008). These models produce a floor in velocity dispersions as a function of SFR that is somewhat lower at higher SFRs ($\gtrsim 10^{-2}$ $M_\odot$ pc^{-2}) that is somewhat below Zhou et al. (2017). However, given the simple structure of our mock galaxies, it is unclear if this is a matter of the dynamical times or ratio of thin to thick stellar disc components being unrealistic, or a problem with the model. Moreover, the general scatter in velocity dispersions agrees with that of the observations, using reasonably inferred parameter values. Lacking outflows, or some sub-grid model for local ISM heating, this model may not correctly capture the leading-edge (in SFR for a given σ_z) of the velocity dispersion relation, where the ISM can be disrupted by outflow events.

Observing the depletion time–stability relation of the mock galaxies in the bottom panel of Fig. 5, the variations (radially) across and between the galaxies affect the normalization of the star formation-turbulence cycles of the individual patches. This results in a widening of the relation within each galaxy, as observed on ∼kpc scales. Galaxy to galaxy variations in gas and stellar properties, and variations in the star formation efficiencies of GMCs, cause the pixel distributions from the mock galaxies to tile the observational space. Though there is still a correlation between the quantities as observed in a single mock galaxy, the correlation is much weaker taken on the whole. Observationally, this may present difficulties in producing a depletion time–stability relation, given that galaxy to galaxy variations in dynamical time and ratios of gaseous and stellar disc scale lengths will result in each galaxy distribution having slightly different normalizations in the depletion time–stability plane, smearing out the signal further through stacking.

Spatially resolved observations of an individual galaxy may indeed see fairly tight correlation between depletion time and Toomre-Q, the exact slope and normalization of which will depend on the disc structure and GMC properties (here, assumed to be related to the 'small-scale' SFE $\langle\epsilon_{sf}\rangle$). However, this is assuming that the star formation parameters are not changing significantly across individual galaxies, e.g. small-scale star formation efficiencies having gas surface density dependencies (Grudić et al. 2018), and again that there are not significant variations in Σ_g between independently evolving ISM patches at constant galactocentric radius.

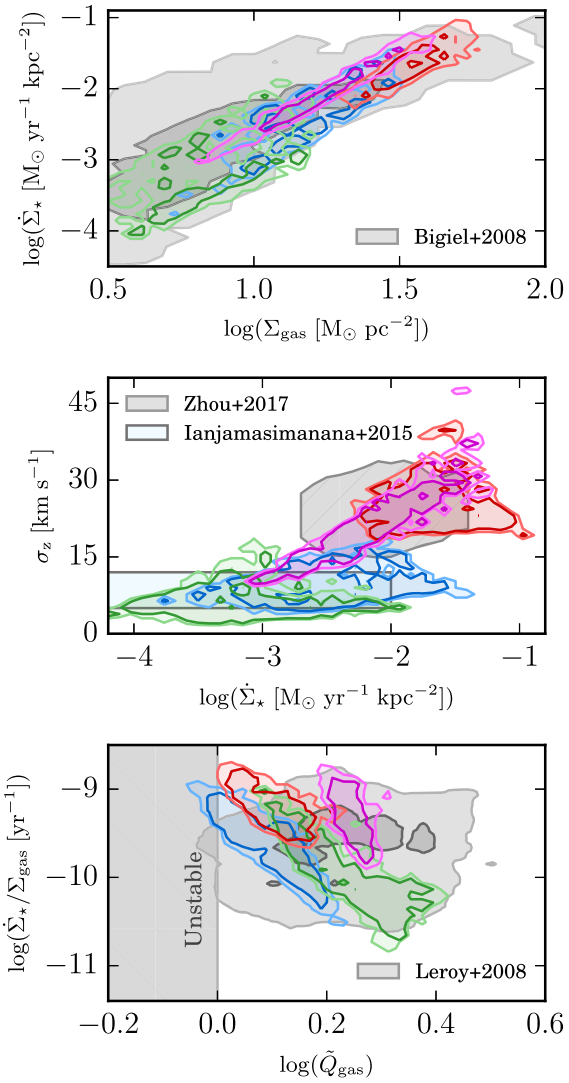

Figure 5. Comparison of the KS, gas velocity and Toomre-Q distributions of the non-equilibrium model (brightly coloured shaded regions) drawn from mock galaxies. Plotted quantities and observational data contours are in the style of Fig. 2. Mock galaxies are exponential profiles of gas and stars, whose properties are summarized in Table 3. The galaxies are sampled at 750 pc resolution for radii $5 < R < 17$ kpc, and a random time-point is chosen in the $3 < \Omega t < 8$ range for the non-equilibrium model with those local conditions. Dark and light shaded regions indicate 50 and 90 per cent inclusion regions for the model pixel distributions. Mock distributions have significant overlap with observations in each panel, and together tile a significant portion of the observational data with modest changes in galaxy properties and star formation efficiencies.

Non-equilibrium SFRs therefore appear to produce an avenue for explaining ∼1-dex scatter in SFRs in the Kennicutt–Schmidt relation, and scatter in the spatially resolved gas velocity dispersion–SFR relation. And although dynamical evolution of star-forming patches may obscure the relation between depletion time and stability somewhat, the variations in the disc properties across and between galaxies are more likely the reason for difficulties

observing a tight correlation between Toomre-Q and SFRs (Leroy et al. 2008).

4 DISCUSSION

4.1 The 'instantaneous' feedback time-scales limit

Much of this work focuses on the case where the feedback delay time-scales $t_{\rm d}$ and $t_{\rm d} + \delta t_{\rm d}$ are within an order of magnitude of the local dynamical time of the galaxy $1/\Omega$ (or for strongly self-gravitating discs, $1/\sqrt{4\pi G\rho_0}$). In the case where $t_{\rm d}$ and $\delta t_{\rm d} \ll 1/\Omega$, however, star formation and feedback can be treated as occurring 'instantaneously' after a delay time $t_{\rm d}$, compressing all SNe and prompt feedback into a spike at $t_{\rm d}$. We too can consider the case when the star formation threshold is very sharp, i.e. $\beta \rightarrow \infty$ such that equation (11) becomes

$$f_{\rm sf}(\tilde{Q}_{\rm gas}) = \theta(Q_0 - \tilde{Q}_{\rm gas}) f_{\rm sf}^0, \tag{13}$$

where $\theta(Q_0 - \tilde{Q}_{\rm gas})$ is the Heaviside step function at the star formation threshold of $\tilde{Q}_{\rm gas} = Q_0$. In this setting, the turbulent velocity dispersion σ is not allowed to fall much below the threshold value at Q_0 since feedback acts effectively instantaneously once star formation begins to occur.

Thus, the amount of star formation that occurs in a star formation episode is just the amount that can form in one feedback time-scale. So, we form an amount of stars per event

$$\Delta\Sigma_\star = \langle\epsilon_{\rm sf}\rangle\ f_{\rm sf}^0 \Sigma_g t_{\rm d}/t_{\rm eddy}\ . \tag{14}$$

Interestingly, the amount of stars formed has no (direct) relation to the absolute strength of feedback, so long as the amount of momentum eventually injected back into the ISM from this mass of stars is enough to at least momentarily halt additional star formation. The time between star formation events is dependent on the fact that each event will pump up the turbulent velocity dispersion by $\Delta\sigma = (P/m_\star)\Delta\Sigma_\star/\Sigma_{\rm g}$. This extra momentum, above that required strictly to maintain stability, takes a time $t_{\rm cycle}$ to decay back down to the star formation threshold $\sigma(\tilde{Q}_{\rm gas} = Q_0)$ of

$$t_{\rm cycle} = \ln(1 + \Delta\sigma/\sigma(\tilde{Q}_{\rm gas} = Q_0))/\,\Omega\ . \tag{15}$$

It is worth noting, that for the outskirts of galaxies, where the quantity $t_{\rm d}\Omega$ is likely to be small as we assumed ($1/\Omega$ being the dominant component of the local dynamical time because of exponentially falling disc surface densities), galaxy discs are seen to have relatively constant H I disc velocity dispersions (Tamburro et al. 2009), and so we expect the ratio of $\Delta\sigma/\sigma(\tilde{Q}_{\rm gas} = Q_0)$ to be small. Thus, we can approximate $t_{\rm cycle}$ as $t_{\rm cycle} \approx \Delta\sigma/\sigma(\tilde{Q}_{\rm gas} = Q_0)\Omega$.

And so the average SFR over a star formation cycle[8] is $\bar{\dot{\Sigma}}_\star = \Delta\Sigma_\star/t_{\rm cycle}$. Explicitly,

$$\bar{\dot{\Sigma}}_\star \approx \frac{\Sigma_{\rm g}\Omega\sigma(\tilde{Q}_{\rm gas} = Q_0)}{P/m_\star}\ . \tag{16}$$

The average efficiency of star formation per dynamical time is then

$$\bar{\epsilon}_{\rm sf} = \frac{\bar{\dot{\Sigma}}_\star}{\Sigma_{\rm g}\Omega} \approx \frac{\sigma(\tilde{Q}_{\rm gas} = Q_0)}{P/m_\star}\ . \tag{17}$$

Neither the average SFR nor the average SFE have an explicit dependence on the 'small scale' (GMC-scale) SFE (here, $\langle\epsilon_{\rm sf}\rangle$) or eddy-crossing/free-fall time $t_{\rm eddy}$, or feedback delay time-scale $t_{\rm d}$ (provided $t_{\rm d}\Omega \ll 1$), so long as the amount of stars formed in a star formation episode injects enough momentum to regulate the ISM but not enough to fully disrupt it (i.e. drive $\tilde{Q}_{\rm gas}$ to $\gg$1). Unsurprisingly, this is identical to the result of Section 2.1, though we are considering a case of extreme dis-equilibrium. This is complementary to the picture of feedback regulation in Semenov et al. (2018), where low star formation efficiencies produce high duty cycles of star formation – after all, less stars formed means $\Delta\sigma/\sigma(\tilde{Q}_{\rm gas} = Q_0)$ will be smaller. Plugging in 'typical' values for $\sigma(\tilde{Q}_{\rm gas} = Q_0) \approx 15$–$45\,{\rm km\,s^{-1}}$ and $P/m_\star \approx 3000\,{\rm km\,s^{-1}}$ yields a global, averaged SFE of $\bar{\epsilon}_{\rm sf} \approx 0.005$–$0.015$. These are not altogether unreasonable values for the SFE in the outskirts of galaxies (Bigiel et al. 2010), and in agreement with the median values of star formation efficiencies of our fiducial model. This provides a reasonable mechanism, reliant on averaging non-equilibrium star formation episodes, for regulating *local* star formation (of any efficiency) to global inefficiency on galactic dynamical time-scales.

4.2 Low gas surface density regime/limit

Seen clearly across the Kennicutt–Schmidt panels of Figs 3 and 4, the delayed feedback model drives large $\sim$2 dex scatter in SFRs for gas surface densities $\lesssim 10\,{\rm M_\odot\,pc^{-2}}$. As the gas surface density falls below $10\,{\rm M_\odot\,pc^{-2}}$, two processes dovetail to make our feedback regulated turbulent disc model break down.

Below $\sim 10\,{\rm M_\odot\,pc^{-2}}$, the gas disc transitions from a supersonic (turbulently supported) molecular disc, to a transonic atomic disc (with non-negligible thermal support), as the sound speed of 6000 K gas is almost but not quite sufficient with $c_{\rm s} \sim 6\,{\rm km\,s^{-1}}$ to maintain $\tilde{Q}_{\rm gas} \sim 1$ (i.e. providing nearly half of the required support). In these circumstances, stirring due to supernovae no longer dominates as the sole process stabilizing the ISM on kpc-scales, and the maintenance of thermal support in a two-phase medium becomes necessary to include. The thermal support component, and its connection to stellar feedback, is not included in the model, as it would require modelling the molecular gas fraction $f_{\rm H_2}$ and gas cooling, which is beyond the scope of this work. Further, given the increasingly two-phase nature of the ISM at low $\Sigma_{\rm g}$, the treatment of the star-forming fraction $f_{\rm sf}(\tilde{Q}_{\rm gas})$ as a simple power law may break down, contributing to a change in kpc-scale star formation efficiencies (Schaye 2004; Krumholz et al. 2009b, 2018). Additional considerations at low gas surface densities include the ability of gas self-gravity (not included) to drive sufficient turbulence in the outer H I discs (Agertz et al. 2009).

On the other hand, for the 'lightest' cold, turbulently supported discs with surface densities $\sim 10\,{\rm M_\odot\,pc^{-2}}$, SNe feedback from star formation events can inject significant fractions of the turbulent momentum in the disc. Take a star formation event at a gas surface density of $10\,{\rm M_\odot\,pc^{-2}}$, where our fiducial model reaches peaks SFRs of $\dot{\Sigma}_\star \sim 10^{-2.5}\,{\rm M_\odot\,kpc^{-2}\,yr^{-1}}$ for $\sim 10^7$ yr (c.f. plausible GMC lifetimes) producing $\sim 10^{4.5}\,{\rm M_\odot\,kpc^{-2}}$ of stars. These young stars then result in an SNe density of $\sim 10^{2.5}\,{\rm kpc^{-2}}$ in the proceeding $\sim$40 Myr (given a rate of a single SNe per $100\,{\rm M_\odot}$ of stars formed; Ostriker et al. 2010). At a momentum per Type II SNe of $\sim 3 \times 10^5\,{\rm M_\odot\,km\,s^{-1}}$ (Martizzi et al. 2015), this is a turbulent momentum injection of $\sim 10^8\,{\rm M_\odot\,km\,s^{-1}\,kpc^{-2}}$. For a $\sim 10\,{\rm M_\odot\,pc^{-2}}$ gas disc, with $\tilde{Q}_{\rm gas} \sim 1$ ($\sigma \sim 10\,{\rm km\,s^{-1}}$), the total turbulent gas momentum is $\sim\Sigma_{\rm g}\sigma(\tilde{Q}_{\rm gas} \sim 1) \sim 10^8\,{\rm M_\odot\,km\,s^{-1}\,kpc^{-2}}$. As the momentum injected is a non-negligible (tens of per cent approaching unity, with uncertainty regarding the feedback budget per SNe Fielding; Quataert & Martizzi 2018; Gentry et al. 2019) fraction of the momentum contained in the turbulence field of the whole disc

[8]This is identical to averaging it over a dynamical time, as then we have a SFR of $\Delta\Sigma_\star\Omega/\Omega t_{\rm cycle} = \Delta\Sigma_\star/t_{\rm cycle}$.

patch, feedback is increasingly disruptive to the disc structure. This is more or less the difference between SNe clusters blowing holes in the ISM (dominating), versus churning or stirring it (perturbations).

And so, given that our model does not capture the feedback, star formation, and gas physics of the transition from a predominantly atomic ISM with non-negligible thermal support to a turbulently supported, molecularly dominated one, this model exhibits increasingly disruptive star formation events at low gas surface densities. It is not clear, on the basis of this model alone, the extent to which growing scatter ($\gtrsim$2 dex) in SFRs due to the time-lag of feedback injection are to be expected for low ($\lesssim 10\,M_\odot\,pc^{-2}$) gas surface density regions. Broadly, this is exemplary of the difficulties in modelling the variety of star formation environments within galaxies with a single, simple model.

5 CONCLUSIONS

In this paper, we developed a simple, non-equilibrium model of star formation in the context of sub-kpc patches of disc galaxies (c.f. local disc scale heights) and explored its ability to explain the scalings and scatter in galaxy star formation relations. Our principal conclusions are as follows:

(i) The local strength of feedback $P/m_\star$, in addition to setting the normalization of the KS relation, itself may contribute to setting the scatter in observed SFRs. If the variance in turbulent momentum is roughly constant through star formation events, then the variance in SFRs is inversely proportional to $P/m_\star$ through $\Delta\sigma \propto P/m_\star \Delta\dot{\Sigma}_\star$.

(ii) Longer delay times between star formation and the injection of feedback t_d and overall injection intervals δt_d are able to drive larger departures from star formation equilibrium. This occurs because the ISM is able to 'overshoot' and overproduce stars to a greater extent, and the subsequent feedback events drive larger velocity dispersions (Toomre-Qs). Delay times on the order of 4–6 Myr produce ∼dex scatter in SFRs.

(iii) The relative steepness of the gravitational instabilities threshold and the time-scale of feedback injection may together explain the large range of SFRs seen at low Σ_g with little variance in velocity dispersions in outer H I disc velocity dispersion profiles (e.g. spiral galaxy H I discs in the THINGS survey; Ianjamasimanana et al. 2012, 2015).

(iv) This model predicts a correlated depletion time–Toomre-Q relation for individual galaxies (c.f. bottom panel of Fig. 5). However, within individual galaxies a degree of scatter is introduced as the normalization and slope of the locally tightly evolving relation varies across discs with the changing disc properties. Further smearing of this relation is introduced in galaxy surveys by stacking different galaxies with altogether different disc and GMC properties (with their attendant differing slopes and normalizations of the depletion time–stability relation).

The proposed non-equilibrium star formation model can explain the observed ∼1 dex scatter in resolved star formation scaling relations. More so than the effects of metallicity or variations in gas fraction, non-equilibrium states of star formation can explain large variations in average SFRs (e.g. Hα-inferred SFRs). This arises due to the fact that the interplay of bursty feedback, injected over some finite time-scale, and the roughly smooth dissipation of turbulence (on ∼kpc scales) struggles to find a stable balance on time-scales of tens of Myrs.

Careful spatially resolved observations of *individual* star-forming galaxies may be able to identify a depletion time–Toomre-Q relation, provided that the effects of variations in gas fraction at constant radius and changes in SFE within GMC across the discs can be accounted for. Indeed, the slope and normalization of this relation may even inform on the small-scale SFE within those specific galaxies.

Future work using resolved galaxy surveys, such as the MaNGA and SAMI surveys, at the sub-kpc scale may help to elucidate the extent to which the scatter in resolved SFRs correlates with dynamical conditions at the disc scale. The ability to marshal statistically significant samples of star-forming regions with similar physical conditions may make it possible to disentangle potentially confounding local quantities such as metallicity or gas fraction.

ACKNOWLEDGEMENTS

MEO is grateful for the encouragement of his late father, SRO, in studying astrophysics. We are grateful to the anonymous referee for providing us with constructive comments and suggestions that greatly improved the quality of this work. MEO is supported by the National Science Foundation Graduate Research Fellowship under Grant No. 1144469. The Flatiron Institute is supported by the Simons Foundation. Support for PFH was provided by an Alfred P. Sloan Research Fellowship, NASA ATP Grant NNX14AH35G, and NSF Collaborative Research Grant #1411920 andCAREER Grant #1455342. This research has used NASA's Astrophysics Data System.

REFERENCES

Agertz O., Kravtsov A. V., 2015, ApJ, 804, 18
Agertz O., Kravtsov A. V., Leitner S. N., Gnedin N. Y., 2013, ApJ, 770, 25
Agertz O., Lake G., Teyssier R., Moore B., Mayer L., Romeo A. B., 2009, MNRAS, 392, 294
Benincasa S. M., Wadsley J., Couchman H. M. P., Keller B. W., 2016, MNRAS, 462, 3053
Bigiel F., Leroy A., Walter F., Blitz L., Brinks E., de Blok W. J. G., Madore B., 2010, AJ, 140, 1194
Bigiel F., Leroy A., Walter F., Brinks E., de Blok W. J. G., Madore B., Thornley M. D., 2008, AJ, 136, 2846
Boehm-Vitense E., 1992, Introduction to stellar astrophysics. Vol. 3 - Stellar structure and evolution. Cambridge University Press, Cambridge
Bolatto A. D., Wolfire M., Leroy A. K., 2013, ARA&A, 51, 207
Calzetti D., Liu G., Koda J., 2012, ApJ, 752, 98
Elmegreen B. G., 2018, ApJ, 854, 16
Elmegreen B. G., Hunter D. A., 2015, ApJ, 805, 145
Evans N. J., Heiderman A., Vutisalchavakul N., 2014, ApJ, 782, 114
Faucher-Giguere C.-A., Quataert E., Hopkins P. F., 2013, MNRAS, 433, 1970
Federrath C. et al., 2017, MNRAS, 468, 3965
Fielding D., Quataert E., Martizzi D., 2018, MNRAS, 481, 3325
Fielding D., Quataert E., Martizzi D., Faucher-Giguère C.-A., 2017, MNRAS, 470, L39
Gallagher M. J. et al., 2018, ApJ, 858, 90
Gentry E. S., Krumholz M. R., Madau P., Lupi A., 2019, MNRAS, 483, 3647
Gilmore G., Reid N., 1983, MNRAS, 202, 1025
Grudić M. Y., Hopkins P. F., Faucher-Giguère C.-A., Quataert E., Murray N., Kereš D., 2018, MNRAS, 475, 3511
Hayward C. C., Hopkins P. F., 2017, MNRAS, 465, 1682
Heyer M., Gutermuth R., Urquhart J. S., Csengeri T., Wienen M., Leurini S., Menten K., Wyrowski F., 2016, A&A, 588, A29
Ho I.-T. et al., 2017, ApJ, 846, 39
Hopkins P. F., 2013, MNRAS, 430, 1653
Hopkins P. F., Kere D., Onorbe J., Faucher-Giguere C.-A., Quataert E., Murray N., Bullock J. S., 2014, MNRAS, 445, 581
Hopkins P. F., Quataert E., Murray N., 2011, MNRAS, 417, 950

Hopkins P. F., Quataert E., Murray N., 2012, MNRAS, 421, 3488
Hopkins P. F. et al., 2018a, MNRAS, 477, 1578
Hopkins P. F. et al., 2018b, MNRAS, 480, 800
Ianjamasimanana R., de Blok W. J. G., Walter F., Heald G. H., 2012, AJ, 144, 96
Ianjamasimanana R., de Blok W. J. G., Walter F., Heald G. H., Caldú-Primo A., Jarrett T. H., 2015, AJ, 150, 47
Kauffmann J., Goldsmith P. F., Melnick G., Tolls V., Guzman A., Menten K. M., 2017, A&A, 605, L5
Kennicutt R. C., Evans N. J., 2012, ARA&A, 50, 531
Kennicutt R. C., Jr. et al., 2007, ApJ, 671, 333
Kim C.-G., Ostriker E. C., 2015a, ApJ, 802, 99
Kim C.-G., Ostriker E. C., 2015b, ApJ, 815, 67
Kim W.-T., Ostriker E. C., 2007, ApJ, 660, 1232
Kruijssen J. M. D., Longmore S. N., 2014, MNRAS, 439, 3239
Kruijssen J. M. D., Schruba A., Hygate A. P. S., Hu C.-Y., Haydon D. T., Longmore S. N., 2018, MNRAS, 479, 1866
Krumholz M. R., 2014, Phys. Rep., 539, 49
Krumholz M. R., Burkhart B., 2016, MNRAS, 458, 1671
Krumholz M. R., Burkhart B., Forbes J. C., Crocker R. M., 2018, MNRAS, 477, 2716
Krumholz M. R., McKee C. F., Tumlinson J., 2009a, ApJ, 693, 216
Krumholz M. R., McKee C. F., Tumlinson J., 2009b, ApJ, 699, 850
Lee E. J., Miville-Deschênes M.-A., Murray N. W., 2016, ApJ, 833, 229
Leitherer C. et al., 1999, ApJS, 123, 3
Leroy A. K., Walter F., Brinks E., Bigiel F., de Blok W. J. G., Madore B., Thornley M. D., 2008, AJ, 136, 2782
Leroy A. K. et al., 2013, AJ, 146, 19
Leroy A. K. et al., 2017, ApJ, 846, 71
Martizzi D., Faucher-Giguere C.-A., Quataert E., 2015, MNRAS, 450, 504
Ma X., Hopkins P. F., Wetzel A. R., Kirby E. N., Anglés-Alcázar D., Faucher-Giguère C.-A., Kereš D., Quataert E., 2017, MNRAS, 467, 2430
McKee C. F., Parravano A., Hollenbach D. J., 2015, ApJ, 814, 13
Murray N., Quataert E., Thompson T. A., 2010, ApJ, 709, 191
Narayanan D., Krumholz M. R., Ostriker E. C., Hernquist L., 2012, MNRAS, 421, 3127
Offner S. S. R., Clark P. C., Hennebelle P., Bastian N., Bate M. R., Hopkins P. F., Moreaux E., Whitworth A. P., 2014, Protostars Planets VI, Vol. 24. University Arizona Press, Tucson, AZ, p. 1
Oklopčić A., Hopkins P. F., Feldmann R., Kereš D., Faucher-Giguère C.-A., Murray N., 2017, MNRAS, 465, 952
Onus A., Krumholz M. R., Federrath C., 2018, MNRAS, 479, 1702
Orr M. E. et al., 2017, ApJ, 849, L2
Orr M. E. et al., 2018, MNRAS, 478, 3653
Ostriker E. C., McKee C. F., Leroy A. K., 2010, ApJ, 721, 975
Ostriker E. C., Shetty R., 2011, ApJ, 731, 41
Padoan P., Pan L., Haugbølle T., Nordlund Å., 2016, ApJ, 822, 11
Rafikov R. R., 2001, MNRAS, 323, 445
Raiteri C. M., Villata M., Navarro J. F., 1996, A&A, 315, 105
Robertson B., Goldreich P., 2012, ApJ, 750, L31
Saitoh T. R., Daisaka H., Kokubo E., Makino J., Okamoto T., Tomisaka K., Wada K., Yoshida N., 2008, PASJ, 60, 667
Schaye J., 2004, ApJ, 609, 667
Schruba A., Leroy A. K., Walter F., Sandstrom K., Rosolowsky E., 2010, ApJ, 722, 1699
Scoville N. Z., Sanders D. B., 1987, in Hollenbach D. J., Thronson H. A., Jr., eds, Astrophysics and Space Science Library, Vol. 134, Interstellar Processes. Reidel, Dordrecht, p. 21
Semenov V. A., Kravtsov A. V., Gnedin N. Y., 2017, ApJ, 845, 133
Semenov V. A., Kravtsov A. V., Gnedin N. Y., 2018, ApJ, 861, 4
Shetty R., Ostriker E. C., 2012a, ApJ, 754, 2
Shetty R., Ostriker E. C., 2012b, ApJ, 754, 2
Smartt S. J., 2009, ARA&A, 47, 63
Sparre M. et al., 2017, MNRAS, 466, 88
Tamburro D., Rix H.-W., Leroy A. K., Mac Low M.-M., Walter F., Kennicutt R. C., Brinks E., de Blok W. J. G., 2009, AJ, 137, 4424
Thompson T. A., Quataert E., Murray N., 2005, ApJ, 630, 167
Toomre A.., 1964, ApJ, 139, 1217
Torrey P., Hopkins P. F., Faucher-Giguère C.-A., Vogelsberger M., Quataert E., Kereš D., Murray N., 2017, MNRAS, 467, 2301
Zhou L. et al., 2017, MNRAS, 470, 4573

APPENDIX A: PARAMETERS OF SUPERNOVA FEEDBACK

The lifetimes of massive (8–40 $M_\odot$) stars that are the progenitors of Type II SNe events are fairly well constrained for our purposes. Furthermore, the slope of the massive end of the stellar initial mass function (IMF) is also well known (see Krumholz 2014; Offner et al. 2014; and references therein). Together, these constraints put a strong prior on the parameter space to be explored by this model, in terms of the delay time to the first effects of SNe feedback being felt, how long feedback events last, and the relative distribution of feedback injection in time after a star formation event.

From stellar evolution theory, the main-sequence lifetimes of the most massive stars in the local Universe range from approximately 4.5 to 38 Myr for 40 to 8 $M_\odot$ stars (Raiteri, Villata & Navarro 1996). We take the lifetime of a 40 $M_\odot$ star as a bound for the minimum delay time to the first SNe feedback effects in our model t_d. Admittedly, longer delay times by perhaps a factor of 2 are not unreasonable given the (un)likelihood of forming the most massive star first in a local star formation episode, in addition to the various effects rotation and binarity. On the other hand, there is a broader absolute range in the time for the last Type II SNe to go off of 30–49 Myr (approximately factor of two uncertainty), given the uncertainty in the lower mass limit for Type II SNe progenitors of $8 \pm 1\,M_\odot$ (Smartt 2009).

To constrain the distribution in time of Type II SNe events from a star formation episode (between the most and least-massive progenitor's endpoints), i.e. $\mathrm{d}N_{\rm SN}/\mathrm{d}t$, we combine the IMF slope $\mathrm{d}N/\mathrm{d}M_\star$ and the mass dependence of main-sequence lifetimes (specifically $\mathrm{d}t/\mathrm{d}M_\star$). Taking the lifetimes of massive stars to be proportional to their mass-to-light ratios $t(M_\star) \propto M_\star/L_\star$ and with $L_\star \propto M_\star^{3.5}$, we have $t(M_\star) \propto M_\star^{-2.5}$ (or $M_\star \propto t^{-2/5}$) and thus $\mathrm{d}M_\star/\mathrm{d}t \propto t^{-7/5}$ (Boehm-Vitense 1992). From the slope of the high-mass end of the IMF, we take the canonical Salpeter IMF slope of −2.35, i.e. $\mathrm{d}N/\mathrm{d}M_\star \propto M_\star^{-2.35}$, and in terms of their stellar lifetimes $\mathrm{d}N/\mathrm{d}M_\star$ is then $\propto t^{4.7/5}$. Combining these arguments, we yield a power-law distribution of

$$\frac{\mathrm{d}N_{\rm SN}}{\mathrm{d}t} = \frac{\mathrm{d}N}{\mathrm{d}M_\star}\frac{\mathrm{d}M_\star}{\mathrm{d}t} \propto t^{-0.46}, \tag{A1}$$

which is fairly weak (though not flat) in time, as the shorter lifetimes of the most massive stars nearly balance out with their relative rarity.

For the purposes of this study, we thus adopt an initial delay time of $t_d = 5$ Myr, a feedback episode period of $\delta t_d = 30$ Myr, and a time-weighting of $\mathrm{d}N_{\rm SN}/\mathrm{d}t \propto t^{-0.46}$.

APPENDIX B: WHAT ABOUT SFR AVERAGING TIME-SCALES?

Observationally, the 'instantaneous' SFR of a region is ill-defined. Young stellar object (YSO) counts are perhaps the closest proxy to a true instantaneous SFR, but even they have a spread in their lifetimes (hence the averaging time-scale of SFRs inferred) of as little as 0.5 Myr for 0/I YSOs to being an Myr or more removed from the star formation event itself in the case of Class II YSOs (Evans, Heiderman & Vutisalchavakul 2014; Heyer et al. 2016). As such, any model of non-equilibrium star formation must be convolved with an averaging time-scale for the observable tracer.

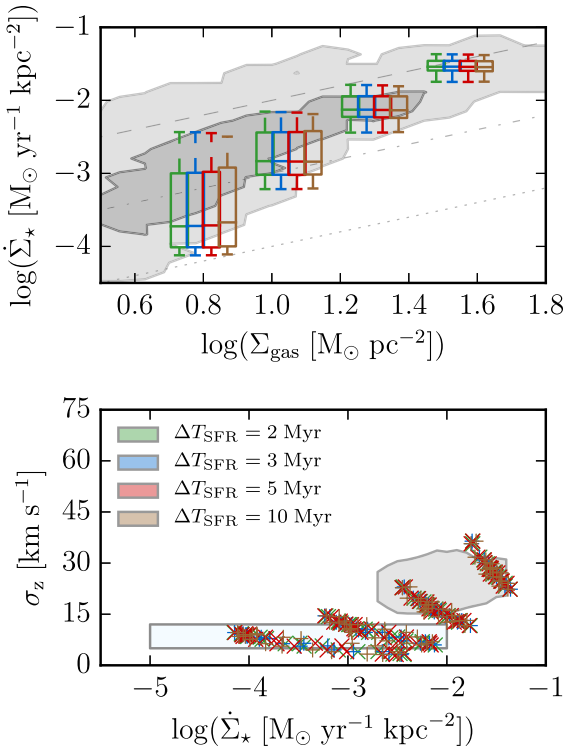

Figure B1. Effects of variation in the star formation averaging period on the model KS and gas velocity dispersions for fiducial model parameters. Observational (KS) data and plotted quantities are in the style of Fig. 3. For reasonable choices of averaging period between 2 and 10 Myr (c.f. the Hα tracer time-scale and time-scales thereabouts), little to no effect is seen on the average SFR distributions.

In the case of Hα or IR flux, we are averaging over a $\sim$2–4 Myr time-scale, for tracers such as the far-ultraviolet (FUV) flux, that time-scale is significantly longer ($\sim$30 Myr). Hence, variability in SFRs on time-scales shorter than the averaging time-scale of the particular tracer investigated will be smoothed out. We investigate the effects of particular choices of averaging period ΔT_{SFR} in Fig. B1, wherein we convolve the instantaneous SFRs produced by our model (equation 12) with a 2–10 Myr wide time-averaging window ΔT_{SFR}. Specifically, choosing this time-scale to be a proxy for the Hα and IR flux-inferred SFRs, to show how the variations in SFR over the cycle are smoothed out. Increasing the averaging window blunts the SFR maxima achieved, as the peak in the star formation cycle is smoothed to some degree. The particular choice of averaging window does not alter the predictions of the model with respect to Σ_{gas} or σ_z. The averaging effects on $\dot{\Sigma}_\star$ are relatively small as $\Delta T_{\mathrm{SFR}}\Omega \sim 0.1$ in our fiducial model, and so the averaging window constitutes only a fraction of a star formation cycle. Throughout the main body of the text, we adopt a canonical 3 Myr averaging window for our star formation tracer for simplicity.

This paper has been typeset from a TEX/LATEX file prepared by the author.